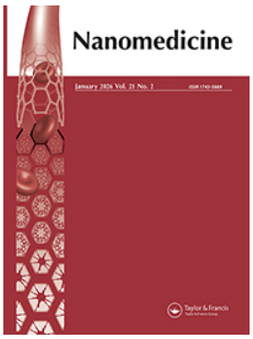

Nanomedicine

ISSN: 1743-5889 (Print) 1748-6963 (Online) Journal homepage: www.tandfonline.com/journals/innm20

Formononetin-derived quantum dots suppress colon cancer growth by triggering mitochondrial apoptosis

Junfeng Zhang, Yuqing Cui, Chenchen Li, Tongjin Yin, Min Xu & Hongliang Bian

To cite this article: Junfeng Zhang, Yuqing Cui, Chenchen Li, Tongjin Yin, Min Xu & Hongliang Bian (12 Jan 2026): Formononetin-derived quantum dots suppress colon cancer growth by triggering mitochondrial apoptosis, Nanomedicine, DOI: 10.1080/17435889.2026.2615097

To link to this article: https://doi.org/10.1080/17435889.2026.2615097

NANOMEDICINE
https://doi.org/10.1080/17435889.2026.2615097

Taylor & Francis
Taylor & Francis Group

RESEARCH ARTICLE

Formononetin-derived quantum dots suppress colon cancer growth by triggering mitochondrial apoptosis

Junfeng Zhang[a*], Yuqing Cui[a*], Chenchen Li[b], Tongjin Yin[c], Min Xu[c] and Hongliang Bian[c]

[a]School of Medicine, Anhui University of Science and Technology, Huainan, P. R. China; [b]School of Pharmacy, Hainan Medical University, Haikou, P. R. China; [c]Department of Pediatrics, Yancheng Third People's Hospital, Affiliated Hospital 6 of Nantong University, Yancheng, P. R. China

ABSTRACT

Formononetin (FMN) is an extracted component of traditional Chinese medicine with anticancer effects, but its poor water solubility and low bioavailability have limited further research and application. Therefore, based on FMN that is the natural antitumor agent, we synthesized a formononetin quantum dots (FMNQDs) for colon cancer therapy, which has the advantages of outstanding water solubility, homogeneous particle size (2.03 ± 1.0 nm), exceptional stability and good intracellular fluorescence imaging effect. The results show that FMNQD exhibits good antitumor activity by inducing mitochondrial-mediated apoptosis, characterized by elevated intracellular reactive oxygen species (ROS) levels, decreased mitochondrial membrane potential (MMP), and modulated expression of Bax and Bcl-2. In *vivo* validation confirmed FMNQD's significant tumor growth inhibition. The tumor inhibition rate in the 8 mg/kg dose group was as high as 60.06 ± 6.22%. Moreover, blood biochemical analysis suggested a favorable safety profile. This study establishes FMNQDs as a potential therapeutic agent for colon cancer, providing preclinical evidence to support further development of formononetin-based nanomedicines.

ARTICLE HISTORY
Received 22 September 2025
Accepted 7 January 2026

KEYWORDS
Formononetin; apoptosis; colon cancer; mitochondria; reactive oxygen species

1. Introduction

Colorectal cancer (CRC) is the third most prevalent and second most lethal cancer worldwide, with high incidence rates and poor clinical outcomes, emphasizing the urgent need for improved treatments [1]. Current management primarily involves surgery, radiation, and chemotherapy [2], but these therapies often come with significant side effects and limited efficacy, especially in advanced stages [3]. Chemotherapeutic agents like 5-fluorouracil (5-FU) and oxaliplatin have been the mainstay of treatment but often fail to provide long-term survival benefits due to toxicity, drug resistance, and low targeting specificity [4]. Therefore, it is urgent to find new antitumor treatment methods. In this context, novel approaches have emerged to address these challenges, including targeted therapies, immunotherapies, and nanomedicine-based solutions.

Recent advancements in novel drug candidates have led to the development of compounds with improved selectivity and reduced side effects, offering new hope for CRC treatment [5,6]. Immunotherapeutic strategies, including immune checkpoint inhibitors and cancer vaccines, have also shown promising results, although immunoevasion mechanisms in CRC present ongoing challenges for effective treatment [7]. Moreover, recent advances in nanomedicine have addressed several limitations of conventional cancer therapies, such as poor bioavailability and low targeting specificity [8,9]. Nanoparticle-based systems offer advantages such as enhanced drug solubility, controlled release, and precise targeting, making them promising candidates for improving cancer treatment outcomes [10]. In particular, quantum dots (QDs) have gained attention due to their optical-electronic properties, high surface area, and multifunctionality, enabling more effective drug delivery and real-time monitoring of CRC treatment, where traditional therapies often fall short [11].

Formononetin (FMN), a bioactive isoflavone, is naturally present in several medicinal botanicals, notably *Trifolium pratense* and *Astragalus membranaceus*, both valued in traditional pharmacopoeias [12]. Over the past 10 years, FMN has emerged as a promising anticancer candidate, with accumulating evidence demonstrating its potent pro-apoptotic and anti-proliferative effects across multiple cancer types [13,14]. Despite demonstrating promising antitumor efficacy, FMN's clinical translation has been significantly limited by several pharmacological challenges, including poor water solubility, inadequate bioavailability, and chemical instability [15]. To overcome these limitations, we developed FMN quantum dots (FMNQDs), a novel nanotherapeutic platform for CRC treatment. The FMNQDs were synthesized through a two-step process involving FMN PEGylation followed by hydrothermal reaction with urea and citric acid (Figure 1(A)), we aimed to enhance FMN's solubility, stability, and targeted drug delivery. The resulting FMNQDs were comprehensively characterized using TEM, UV-vis spectroscopy, fluorescence spectroscopy, and FTIR analysis to confirm their structural and functional properties. To assess their antitumor

CONTACT Hongliang Bian 1002282928@qq.com; Min Xu 15189301103@163.com Department of Pediatrics, Yancheng Third People's Hospital, Affiliated Hospital 6 of Nantong University, Yancheng 224051, P. R. China
*These authors contributed equally to this work.

Supplemental data for this article can be accessed online at https://doi.org/10.1080/17435889.2026.2615097

Article highlights

- FMNQDs Synthesis: Formononetin quantum dots (FMNQDs) were synthesized to overcome FMN's poor water solubility and low bioavailability for colon cancer therapy.
- Outstanding Properties: FMNQDs exhibit excellent water solubility, homogeneous particle size (2.03 ± 1.0 nm), and exceptional stability.
- Mitochondrial-Mediated Apoptosis: FMNQDs induce tumor cell death by triggering mitochondrial-mediated apoptosis and autophagic pathways.
- ROS Production: FMNQD treatment increases intracellular ROS production, a key mechanism in its anticancer activity.
- Tumor Growth Inhibition: FMNQDs show a significant tumor inhibition rate of 60.06 ± 6.22% at 8 mg/kg in colon cancer xenograft models.
- Safe and Biocompatible: FMNQD treatment demonstrates favorable safety profiles, with no observed toxicity in blood biochemical analysis.
- Autophagy Markers: FMNQDs modulate key autophagy markers, increasing LC3-II expression and decreasing p62 expression.
- Future Directions: Future research should explore FMNQD combination therapies and investigate their potential in targeted drug delivery systems for personalized cancer treatment.

efficacy, we evaluated the anticancer mechanism in SW620 human colon carcinoma cells in *vitro*, examining their effects on tumor cell proliferation. In addition, we conducted in *vivo* experiments using xenograft mouse models to evaluate the therapeutic efficacy of FMNQDs. This study presents a novel approach that not only improves the pharmacokinetics of FMN but also provides a powerful tool for CRC treatment. We demonstrate that FMNQDs exhibit significant antitumor activity in both in *vitro* and in *vivo* models, offering a promising strategy for overcoming the current limitations of CRC therapies.

2. Materials and methods

2.1. Materials

Formononetin (CAS No.:485–72-3, Purity: 99%) was provided by Sinopharm Chemical Reagent Co., Ltd. (Shanghai, China). Polyethylene glycol 400 (PEG-400, CAS No.:25322–68-3, Purity: average Mn 400), citric acid (CAS No.:77–92-9, Purity: 99.8%), urea (CAS No.:57–13-6, Purity: 99.8%), and NaOH (CAS No.:1310–73-2, Purity: 99.8%) were obtained from Macklin Biological Technology Co., Ltd. (Shanghai, China).

2.2. Synthesis of FMNQD

FMNQD was prepared by hydrothermal synthesis. Briefly, 1 g FMN was mixed with polyethylene glycol 400 (PEG-400,10 mL), then 20 mL urea solution (0.1 mol/L) was added and stirred by sonication for 10 min. Subsequently, citric acid solution (10 mL, 0.5 mol/L) was slowly added at 60°C and 1000 rpm, and the reaction was condensed and reflux for 6 h. After the reaction, the mixture was pumped and filtered, and 15 mL NaOH solution (0.1 mol/L) was added to the filtrate, and the reaction was heated and stirred for 1 hour (h). The reaction solution was then transferred to a 100 mL Teflon-lined stainless-steel autoclave, and the reaction was hydrothermal for 6 h at 200°C. When the reaction was cooled to room temperature, the solution changed from colorless to brown, indicating the formation of FMNQD. After that, the solution was centrifuged at 10,000 rpm for 10 minutes (min) to remove the precipitate, the supernatant was filtered through a 0.22 μm organic membrane, and the resulting product was dialyzed with ultra-pure water for 24 h (the dialyzate was changed every 6 h) to remove impurities. Finally, the FMNQD samples were freeze-dried.

2.3. Characterization methods

A total of 10 μL FMNQD (30 mg/L) solutions were dripped onto carboncoated 400mesh copper grids by pipette gun and airdried for 24 h to prepare the sample for transmission electron microscopy (TEM; Hitachi, Ltd.) observation. Fourier transform infrared spectroscopy (FTIR) analysis of the dried samples was conducted using Nicolet Avatar370 spectrometer (Thermo Fisher Scientific, USA) across the spectral range of 4000–500 cm^{-1}. The ultraviolet (UV)visible (vis) absorption and fluorescence spectra were measured using UV spectrophotometer (U-3010; Hitachi, Ltd.) and fluorescence spectrophotometer (F-70000; Hitachi, Ltd.), respectively. The quantum yields (QYs) of FMNQD aqueous solutions were determined by comparing the integrated photoluminescence (PL) intensities (excited at 375 nm) and the absorbency values (at 375 nm) using quinine sulfate (QY: 0.55) in sulfuric acid (0.1 mol/L, $\eta = 1.33$) as a reference.

2.4. Cell culture

The human colon carcinoma cell line (SW620) was obtained from the Cell Bank of Chinese Academy of Sciences. Cells were cultured in DMEM (Gino Biological) supplemented with 10% FBS, and maintained at 37°C in a humidified 5% CO_2 incubator.

2.5. Cellular uptake

SW620 cells were cultured in confocal laser scanning microscope (CLSM) dishes. When the cells were adherent and about 60%-70% of the bottom of the dish was covered, the medium was removed, the dish was washed with PBS for 2–3 times, and then 100 mg/mL FMNQD was added to incubate the cells for different times (5, 15, 30, and 60 min), and each time point was repeated three times. After the incubation time, the medium was discarded, and 0.5 mL PBS was added to observe by CLSM.

2.6. Subcellular localization of FMNQD

Following overnight culture of SW620 cells, FMNQD solution (0.2 mg/L) was introduced into the culture medium. To investigate the subcellular localization of FMNQD, we performed co-staining with lysosomal dye (LysoTracker Red), cell membrane dye (Cell Mask) and mitochondrial dye (Mito-Tracker). All the staining reagents were purchased from Beyotime Biotechnology Co., Ltd. (Shanghai, China) and all staining procedures strictly followed manufacturer protocols prior to CLSM analysis.

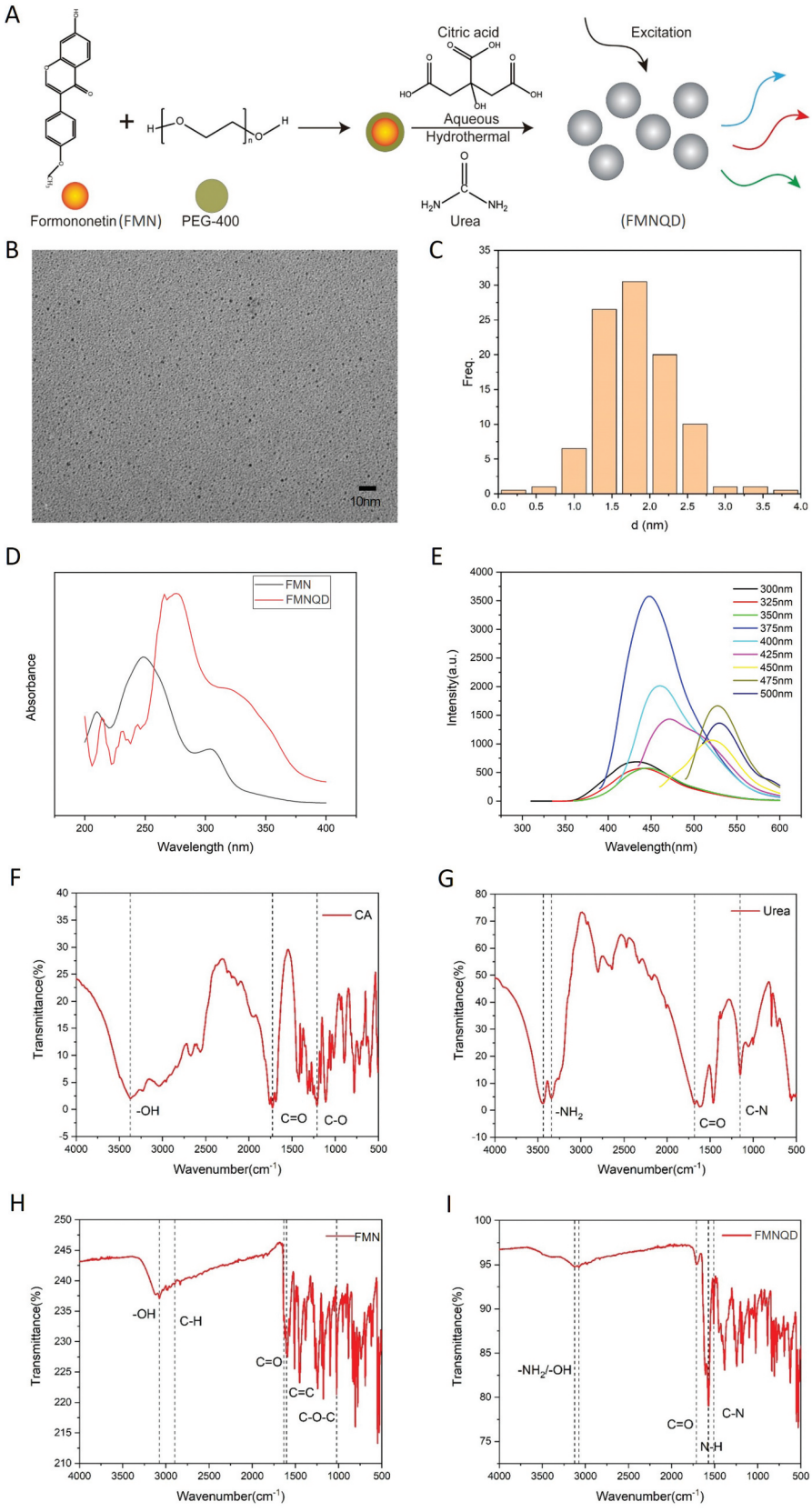

Figure 1. A) Schematic of the preparation process of FMNQD. B) TME imaging of FMNQD, scale bar is 10 nm. C) Particle size distribution of FMNQD. D) UV-vis spectra of FMNQD. E) Fluorescence spectra of FMNQD. F) FTIR spectra of citric acid. G) FTIR spectra of urea. H) FTIR spectra of FMN. I) FTIR spectra of FMNQD.

Abbreviations: FMN, formononetin; FMNQD, formononetin quantum dot; CA, citric acid.

2.7. In vitro cytotoxicity

The cytotoxic effects of FMNQD were assessed with CCK-8 assay. SW620 cells were seeded in 96-well plates (5×10^3 cells/well). After incubation overnight, the medium was replaced and fresh medium containing FMNQD (0, 50, 100, 150, 200, 300 μg/mL) and FMN (0, 50, 100, 150, 200, 300 μ g/mL) were added to the plates at different time points (12, 24 h). We also evaluated the cytotoxicity of FMNQD and 5-FU using the CCK-8 assay on SW620 cells. Cells were treated with varying concentrations of FMNQD (0, 100, 200, 300 μg/mL) and 5-FU (0, 1.5, 3, 6 μg/mL) for 24 hours. Then, cell viability was determined by CCK-8 kit (Beyotime, Shanghai, China) according to standard protocols.

2.8. Intracellular ROS detection

Intracellular ROS levels in SW620 cells were assessed using DCFH-DA fluorescent probe. Cells were treated with FMNQD solution (0, 100, 200, 300 mg/L) for 12 hours, followed by ROS detection using ROS Assay Kit (Beyotime, Shanghai, China). Following the manufacturer's protocol, DCF fluorescence was quantified through CLSM to evaluate ROS production. Additionally, the cells were treated with FMNQD solutions (0, 100, 200, 300 mg/L) and free FMN (0, 100, 200, 300 mg/L) for 12 hours, and the generation of ROS was detected by flow cytometry.

2.9. Detection of mitochondrial membrane potential (MMP)

MMP was monitored using JC-1 fluorescent probe (Beyotime, Shanghai, China). Following 12 hours treatment with FMNQD solution (100 mg/L) and free FMN solution (100 mg/L), cells were stained with JC-1 for 20 minutes and analyzed by CLSM. The excitation wavelength of 488 nm was selected for the JC-1, and the emission wavelength of JC-1 monomer and JC-1 aggregate were set to 515–545 nm and 570–600 nm, respectively.

2.10. Cell apoptosis

Cell apoptosis was quantified using Annexin V-FITC/PI Apoptosis Detection Kit (Beyotime, Shanghai, China). After culturing cells with FMNQD solution (100 mg/L) and FMN solution (100 mg/L) for 12 h, the cells were processed according to the protocol of the kit and analyzed by flow cytometry. Each experiment was performed in triplicate.

2.11. Quantitative real-time PCR analysis

Gene expression levels of Bax, Bcl-2, c-Myc, caspase-3, cytochrome c, LC3-II, and p62 were quantified using qRT-PCR (Beyotime, Shanghai, China). Total RNA was extracted from SW620 cells using Trizol reagent according to the manufacturer's instructions. GAPDH was used as the housekeeping gene for normalization. The primer sequences are provided in Table 1. The qRT-PCR analysis was performed using the SYBR Green method, and data were analyzed using the $2^{-\Delta\Delta Ct}$ method.

2.12. Therapeutic effect in Vivo

The 36 female BALB/c-nude mice (aged 6–8 weeks, with an average weight of 20–22 g) from Jiangsu Laboratory Animal Center. The mice were housed in standard plastic cages with appropriate bedding, and each cage contained 3 mice. The room temperature was maintained at 22 ± 2°C, with a 12-hour light/dark cycle [16]. Mice had free access to food (standard laboratory chow) and water. The animal facility was kept under controlled conditions to ensure animal welfare and minimize stress. Every effort was made to reduce animal suffering, including monitoring animals daily for signs of distress, and providing proper anesthesia during surgical procedures and euthanasia. The mice were subcutaneously inoculated with SW620 cells (1×10^7 cells/100 μL) in the right flank. Upon reaching tumor volumes of ~100 mm^3, mice were randomized into six treatment groups (n = 6/group): control (normal saline), FMNQD low-dose (2 mg/kg), FMNQD medium-dose (5 mg/kg), FMNQD high-dose (8 mg/kg), FMN (8 mg/kg), and 5-FU (20 mg/kg). The FMN, FMNQD and 5-FU solutions were administered via tail vein injection every 3 days for 27 consecutive days. The dose volume for each injection was 200 μL. Tumor size and body weight were monitored every 3 days during the treatment period. At the end of the experiment, mice were euthanized by cervical dislocation following anesthesia with isoflurane, and the final weight of their tumors was recorded. All experiments complied with China's national laboratory animal welfare guidelines and were approved by the Institutional Animal Care and Use Committee of Anhui University of Science and Technology (S22024014).

2.13. Evaluation of toxicity in Vivo

Blood samples were processed by centrifugation (3000 rpm, 5 min) for serum collection. Liver function was assessed through ALT, AST, and ALP quantification, while kidney toxicity was evaluated by measuring CRE, UREA, and UA levels. All analyses

Table 1. Primer sequences used for real-time PCR.

Genes	Forward primer (5′-3′)	Reverse primer (5′-3′)
Bax	TTGCTACAGGGTTTCATCCAGG	GCAAAGTAGAAGAGGGCAACCA
Bcl-2	CTACCGTCGTGACTTCGCAGA	ACACATGACCCCACCGAAC
c-Myc	CCTTCTCTCCTTCCTCGGACT	TGCCTCTTCTCCACAGACACC
Caspase-3	TGGAAAGCCGAAACTCTTCATCA	CCACGACCCGTCCTTTGAAT
Cytochrome c	GGTCAACAAATCATAAAGATATTGG	TAAACTTCAGGGTGACCAAAAAATCA
LC3-II	ATGCCGTCGGACAAGACCTT	TTACACTGACAATTTCATCCCG
p62	TGCCCAGACTACGACTTGTG	AGTGTCCGTGTTTCACCTTCC
GAPDH	GGTGAAGGTCGGAGTCAACG	CTCGCTCCTGGAAGATGGTG

were performed using commercial assay kits (Beyotime, Shanghai, China) according to the manufacturer's protocols.

To evaluate the pharmacokinetic properties of FMNQDs, we measured the absorbance of different concentrations of FMNQDs at 271 nm using a UV-Visible spectrophotometer and plotted the corresponding UV standard curve (Figure S1A). We injected FMNQDs into healthy mice and collected blood samples at different time points after the injection. The samples were centrifuged at 3000 rpm for 10 minutes to obtain the supernatant. The absorbance at 271 nm was measured using a UV-Visible spectrophotometer. Then, the concentration of FMNQDs in the mice's blood at different time points were determined using a UV standard curve. In addition, the relative pharmacokinetic data were obtained from the PKsolver 2.0 software.

To assess the metabolism and clearance of FMNQDs, we collect urine samples from mice at different time points following intravenous injection of FMNQDs. To ensure consistency, the urine volumes will be adjusted to the same final volume for each time point. The concentration of FMNQDs in the urine will be determined using a UV absorbance standard curve, which was previously established based on known concentrations of FMNQDs. By quantifying the FMNQD levels in urine over time, we will be able to assess the clearance of FMNQDs from the body.

2.14. Statistical analysis

The data were presented as mean ± SEM. Statistical analyses were conducted using GraphPad Prism version 8.0 (GraphPad Software, La Jolla, CA, USA). One-way analysis of variance (ANOVA) followed by Tukey's post hoc test was used to compare multiple groups, while Student's t-test was applied for comparisons between two groups. Significance levels were defined as $*p < 0.05$, $**p < 0.01$ and $***p < 0.01$.

3. Results

3.1. Characterization of FMNQD

The particle sizes of FMNQD were assessed using TEM (Figure 1(B)). FMNQD had good dispersibility, and most of them were in a monodisperse state with a particle size of 2.03 ± 1.0 nm, and the size distribution was calculated based on measurements from a total of 100 individual particles, analyzed using ImageJ software (Figure 1(C)). To assess the stability of FMNQDs in solution, we performed Dynamic Light Scattering (DLS) and zeta potential measurements. The results showed a hydrodynamic size distribution of 6.21 nm (Figure S2A), and the zeta potential of FMNQDs was −18.72 mV (Figure S2B), indicating good stability in solution. UVvis spectra demonstrated notable absorbance of FMN at 250 nm and of FMNQD at 271 nm, which may be due to the change in the molecular structure of formononetin compounds (Figure 1(D)). In addition, the fluorescence intensity of FMNQD was investigated at different excitation wavelengths (300, 325, 350, 375, 400, 425, 450, 475, and 500 nm) in the range of 300–500 nm. The results showed that the fluorescence intensity of FMNQD was the strongest when the excitation wavelength was 375 nm, and the emission peak occurs at 450 nm at this time (Figure 1(E)), with a quantum yield of up to 28.3%. In addition, we performed a photostability test under prolonged excitation. The FMNQDs were excited continuously at 375 nm for 10 minutes, and their fluorescence intensity was measured. The results showed that the fluorescence intensity of FMNQDs remains stable, confirming their good photostability, which is ideal for imaging applications (Figure S3). We also tested the fluorescence emission of FMNQDs in PBS and serum. The emission spectrum of FMNQDs was measured after incubation in PBS and serum to simulate in vivo conditions. The results show that the fluorescence intensity of FMNQDs remains stable in biological media, suggesting that they will perform well in in vivo imaging (Figure S4).

After that, we studied the FTIR spectra of citric acid, Urea, FMN and FMNQD (Figure 1(F-I)). For FMN, the spectrum displays an -OH stretch at 3075 cm^{-1}, consistent with its phenolic group, and C-H stretching vibrations at 2897 cm^{-1} (for both alkyl and aromatic groups). The C = C bond stretching in the aromatic ring is observed at 1604 cm^{-1}, and characteristic C = O and C-O-C stretching vibrations appear at 1633 cm^{-1} and 1025 cm^{-1}, respectively. For Urea spectrum, N-H stretching vibration at 3343 and 3438 cm^{-1} and C = O stretching vibration at 1682 cm^{-1} could be observed. For citric acid, the broad peak from 2500 to 3500 cm^{-1} corresponds to the O-H stretching vibrations, while the C = O stretching of the carboxyl group appears at 1729 cm^{-1}. The C-O and C-H bond stretching vibrations are found between 1200 and 1400 cm^{-1}. In the FMNQD spectrum, the peak in the range of 3000 to 3200 cm^{-1} indicates the possible presence of an -OH group. Additionally, a significant peak around 1573 cm^{-1} is attributed to the N-H bond, suggesting the presence of amine functional groups. The shift of the C = O stretching peak from 1633 cm^{-1} (in FMN) to 1715 cm^{-1} in FMNQD provides strong evidence for amide bond formation between FMN and citric acid/urea during the synthesis [17]. The formation of amide bonds likely enhances the stability and bioavailability of FMN, potentially increasing its antitumor efficacy by improving its aqueous solubility and facilitating better cellular uptake [18,19].

We analyzed the fluorescence stability of FMNQD at different concentrations, different pH solutions and different ionic solutions. As the FMNQD concentration increased from 0.1 mg/mL to 2 mg/mL, the fluorescence intensity showed a trend of first increasing and then decreasing. We noted that at the 2 mg/mL, the fluorescence intensity of FMNQD was almost zero. This may be because the high concentration leads to the strengthening of the self-absorption effect, which in turn leads to fluorescence quenching. The results showed that the maximum fluorescence intensity was obtained when the mass concentration of FMNQD was 0.2 mg/mL (Figure 2(A)).

To further investigate the sensitivity of the fluorescence intensity of FMNQD to the pH of the medium, the fluorescence intensity changes in different solutions with pH = 1 to 12 were investigated. The results show that the fluorescence intensity of the FMNQD is higher in alkaline conditions than in acidic conditions (Figure 2(B)). The fluorescence intensity of FMNQD is the highest within the pH range of 7 to 8 (a slightly alkaline environment). The reason for this phenomenon may be is likely due to the surface interactions of FMNQD, which are

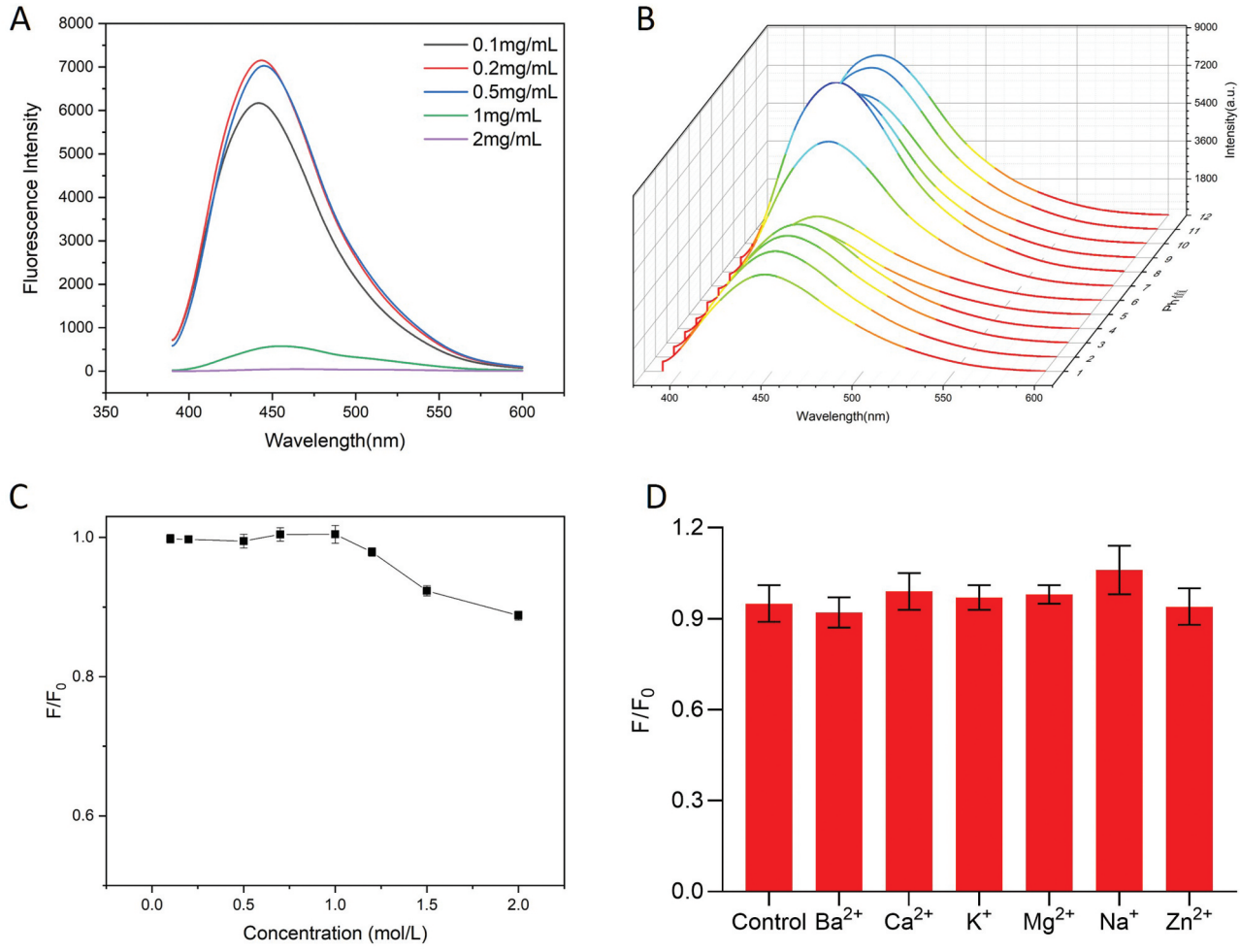

Figure 2. A) Fluorescence intensity of FMNQD at different concentrations. B) The effect of different pH values on the fluorescence intensity of FMNQD. C) The effect of different concentrations of NaCl on the fluorescence intensity of FMNQD. D) The effect of different ions on the fluorescence intensity of FMNQD.

optimized in this slightly alkaline environment. At lower pH (acidic conditions), aggregation and self-quenching occur due to changes in the surface functional groups, leading to a decrease in fluorescence intensity. We have also tested the fluorescence of FMNQDs across a pH gradient ranging from 6.5 to 7.4, which simulates in vivo conditions in the tumor microenvironment. The results show that FMNQDs maintain high fluorescence intensity in this range, which supports their potential for use in biological applications (Figure S5).

We investigated the effect of NaCl solutions on the fluorescence intensity of FMNQD. We added an equal volume of FMNQD solution (0.2 mg/mL) to NaCl solution (0.1–2 mol/L) and determined the fluorescence intensity of different samples at an excitation wavelength of 375 nm. The results showed that in the range of 0.1–1.0 mol/L NaCl solution, the fluorescence intensity of FMNQD had little effect, and in the range of 1–2 mol/L NaCl solution, the fluorescence intensity of FMNQD decreased slightly, but it was still in the relatively high fluorescence intensity range (Figure 2(C)). This indicates that FMNQD is less affected by NaCl solution and can maintain better fluorescence stability. We conducted additional measurements to evaluate the effect of ionic strength on particle size and zeta potential. The results showed that FMNQD maintained a stable size and zeta potential within the range of 0.1–1.0 mol/L NaCl, indicating that FMNQD is relatively stable in solutions with ionic strengths up to physiological levels (Figure S6).

Furthermore, the effects of different metal cations on the fluorescence stability of FMNQD were investigated. The same volume and concentration of FMNQD solution was added to Ba^{2+}, Ca^{2+}, K^{+}, Mg^{2+}, Na^{+}, and Zn^{2+} ion solutions at a concentration of 1 mmol/L, respectively. The fluorescence intensity was measured at 375 nm excitation wavelength. The solution with the same volume of deionized water was used as the control group. The results showed that after adding these metal cations, the relative fluorescence intensity mostly remained above 0.9, indicating that FMNQD can exist stably in various metal ions and has good stability and resistance to external ion interference (Figure 2(D)). To further assess the potential for metal ion interference, we performed competition assays using biological chelator such as EDTA. The EDTA (5 mmol/L) was added to FMNQD solutions in the presence of metal ion (Zn^{2+}) to evaluate if they affect the fluorescence stability of FMNQDs. The results showed that FMNQDs maintain fluorescence stability even in the presence of metal ion chelators, suggesting that FMNQDs are not

interfered with by metal ions when targeting specific cellular structures, such as the mitochondria (Figure S7).

3.2. Cellular uptake and subcellular localization of FMNQD

We incubated FMNQD with SW620 cells for different times (5, 15, 30, and 60 min) and observed the cells by CLSM. The results showed that the intracellular fluorescence intensity gradually increased with the time of incubation of cells with FMNQD, and FMNQD was taken up by cells and distributed in the cytoplasm, thereby achieving transmembrane transfer (Figure 3(A)). The quantitative analysis clearly indicates a gradual increase in fluorescence intensity, reflecting the time-dependent internalization of FMNQDs (Figure S8). We used endocytosis inhibitors (such as chlorpromazine and cytochalasin) to investigate the internalization mechanism of FMNQDs. These inhibitors specifically inhibited the clathrin-mediated and caveolae-mediated endocytosis, respectively. The results show that the FMNQD uptake was significantly reduced in the presence of these inhibitors, suggesting that FMNQDs are primarily internalized via clathrin-mediated endocytosis (Figure S9). Then, we then investigated the intracellular colocalization of FMNQD. The Pearson's coefficient for colocalization with mitochondria was found to be 0.79, and for lysosomes, it was 0.89. The results show that FMNQD can enter the cell through the cell membrane and is distributed in the cytoplasm, partly near mitochondria but mostly near lysosomes (Figure 3(B)).

3.3. In vitro cytotoxicity and intracellular ROS detection

We assessed the cell viability using CCK-8 assay, and the results of the study showed that the cell viability gradually decreased with the increase of the concentration, both after 12 h and after 24 h treatment (Figure 4(A,B)). The IC50 values for FMNQD were found to be 771.5 μg/mL at 12 h and 213.3 μg/mL at 24 h, while the IC50 values for FMN were 1541 μg/mL at 12 h and 1352 μg/mL at 24 h. These results further highlight the stronger cytotoxicity of FMNQDs compared to FMN, likely due to the enhanced cellular uptake and

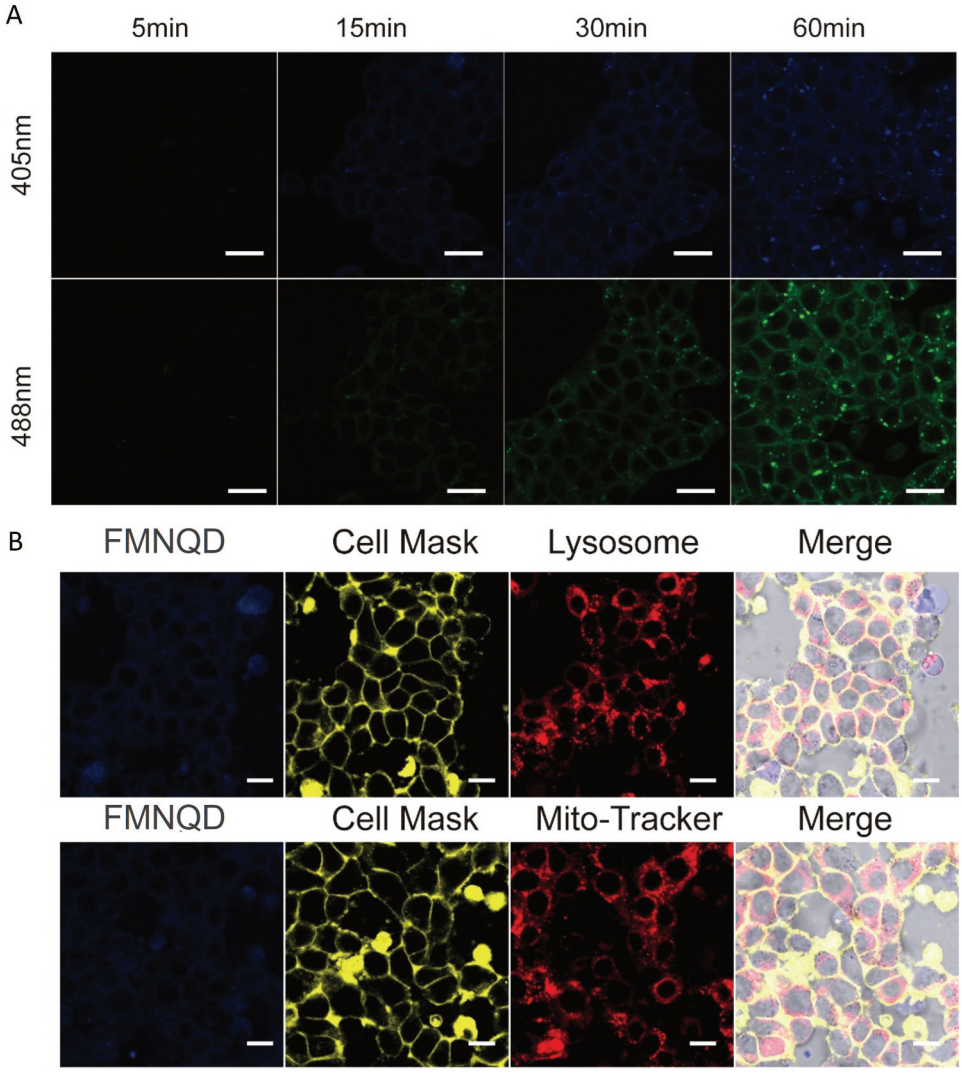

Figure 3. A) Distribution of FMNQD uptake by cells at different times at two excitation wavelengths (405 nm and 488 nm). B) Intracellular colocalization experiments of FMNQD.

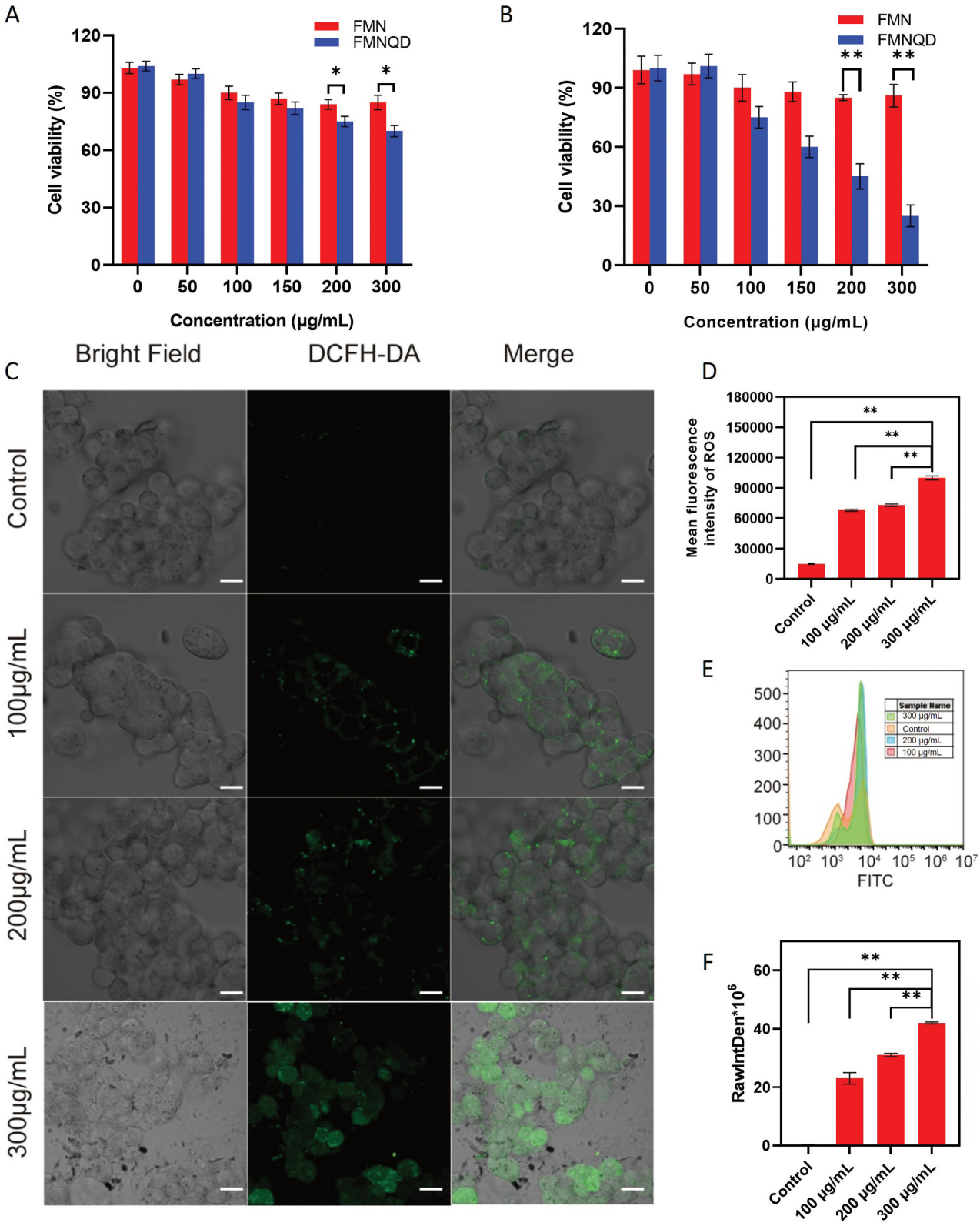

Figure 4. Cytotoxicity of SW620 cells incubated with the FMN and FMNQD for different times at different concentrations: A) 12 h, B) 24 h. n = 6 per group. C) Fluorescence images of ROS produced after different treatments of SW620 cells by CLSM. Scale bar, 20 μm. D) Semiquantitative fluorescence analysis of ROS produced. E) The effect of different concentrations of FMNQD on the content of ROS in SW620 was measured by flow cytometry. F) The distribution of intracellular ROS. n = 3 per group. $^{**}p < 0.05$, $^{*}p < 0.01$.

bioavailability of FMNQDs. In addition, FMNQD exhibited a stronger cytotoxic effect than 5-FU at the same time points (Figure S10). Specifically, FMNQD demonstrated superior cell viability inhibition at 24 hours, likely due to its enhanced bioavailability and nanoparticle formulation, which allows for more efficient cellular uptake and increased drug delivery. These results suggest that FMNQD has a more potent anti-tumor activity than FMN and 5-FU in the in *vitro* model. We

also tested the selectivity of FMNQDs for non-cancerous colon cells (CCD-18Co cells, a normal colon fibroblast cell line). The results show that FMNQDs exhibit significantly lower cytotoxicity against CCD-18Co cells compared to SW620 cancer cells, supporting the selective cytotoxicity of FMNQDs toward cancer cells (Figure S11). This indicates that FMNQDs have enhanced selectivity for tumor cells, which is an important feature for reducing off-target effects and minimizing toxicity to normal tissues. To test the efficacy of FMNQD in different colon cancer cell lines, we conducted a cytotoxicity assay using HCT116 cells. The results from the HCT116 cytotoxicity assays were consistent with our findings in SW620 cells, further supporting the antitumor efficacy of FMNQDs (Figure S12).

Intracellular ROS levels were assessed using the DCFH-DA fluorescent probe, with DCF fluorescence visualized by confocal laser scanning microscopy CLSM. The results demonstrated that FMNQD-treated SW620 cells exhibited markedly enhanced green fluorescence compared to untreated controls, which showed negligible signal (Figure 4(C)). Quantitative analysis revealed significantly elevated ROS levels in FMNQD-treated cells relative to controls (Figure 4(D)). In addition, we also measured the intracellular ROS content by flow cytometry, and the results show that free FMN treatment also leads to an increase in ROS levels compared to untreated controls, but the increase is less pronounced compared to FMNQD treatment (Figure 4(E,F), S13). This highlights the enhanced ROS generation induced by FMNQD, likely due to the increased bioavailability and uptake facilitated by the quantum dot formulation.

3.4. Cell apoptosis and detection of mitochondrial membrane potential (MMP)

The apoptotic effects of FMNQD and FMN on SW620 cells were evaluated using annexin V-FITC/PI staining combined with flow cytometry. The apoptosis rate of SW620 cells with FMNQD was 81.86 ± 2.27%, which was significantly higher than that of cells in the control group (5.42 ± 0.21%) and FMN group (27.79 ± 1.57%), indicating that FMNQD significantly increased the apoptosis of SW620 cells (Figure 5(A,B)). In addition, qRT-PCR analysis demonstrated FMNQD upregulated pro-apoptotic Bax and caspases-3 levels while downregulating anti-apoptotic Bcl-2, and suppressing proliferation-associated c-Myc expression relative to controls (Figure 5(C–E), S14A).

We evaluated the changes of MMP in FMNQD-treated and free FMN-treated SW620 cells using JC-1 staining. This fluorescent probe differentially localizes based on MMP status: forming red-fluorescent aggregates in healthy cells with preserved MMP, while existing as green-fluorescent monomers when MMP declines. Fluorescence imaging revealed intense red signals in untreated controls, contrasting with FMNQD-treated cells that displayed diminished red fluorescence and concurrent green signal intensification (Figure 5(F)). Fluorescence semi-quantitative results showed that the ratios of JC-1 aggregate/JC-1 monomer in the control and FMNQD groups were 52.36 ± 2.65 and 23.75 ± 4.27, respectively (Figure 5(G)), and for the free FMN group, the ratio was 43.23 ± 3.26 (Figure S15). The results demonstrate that while free FMN treatment leads to a reduction in MMP (similar to FMNQD treatment), the extent of the reduction is more pronounced with FMNQD, suggesting that the quantum dot formulation enhances the ability of FMN to induce mitochondrial dysfunction. We had assessed the release of cytochrome c from the mitochondria into the cytosol, a key step in mitochondrial-mediated apoptosis. Our results showed that FMNQD treatment significantly enhanced cytochrome c release, further supporting the involvement of mitochondrial dysfunction in FMNQD-induced apoptosis (Figure S14B).

In addition to apoptosis markers, we had also examined the autophagic flux by measuring the expression levels of LC3-II and p62, both of which are well-established markers of autophagy. Our results indicated that FMNQD treatment led to an increase in LC3-II expression, suggesting the induction of autophagic activity (Figure S14C). We also observed a decrease in p62, further confirming the activation of autophagy (Figure S14D).

3.5. Therapeutic effect in vivo

To evaluate the in *vivo* anti-tumor efficacy of FMNQD, treatment was initiated when the tumor reached 100 mm^3. The FMNQD and FMN treatments were administered via tail vein injection every 3 days for 27 consecutive days. Compared with the control group, the tumor growth rates in the FMNQD treatment groups were significantly inhibited (Figure 6(A), S16A). Tumor inhibition rates were 29.36 ± 3.74% (2 mg/kg FMNQD), 47.31 ± 4.91% (5 mg/kg FMNQD), 60.06 ± 6.22% (8 mg/kg FMNQD), 28.14 ± 4.01% (8 mg/kg FMN), and 40.12 ± 4.83% (20 mg/kg 5-FU) (Figure 6(B), S16B). Three days after the last treatment, the mice were sacrificed and tumor tissues were weighed. Tumor weights in the 5 mg/kg and 8 mg/kg FMNQD groups were significantly reduced compared to the control and FMN groups (Figure 6(D)). Body weight data showed stability across treatment groups during the study, indicating no overt toxicity from FMNQD (Figure 6(C)). These results confirmed the enhanced antitumor efficacy of FMNQD relative to FMN and 5-FU.

3.6. Biosafety and toxicity in vivo

At the end of the treatment, the analysis of serum biomarkers for the liver (ALT, AST, ALP) and the kidney (CRE, UREA, UA) showed that their levels were not significantly different from those of the control group (Figure 6(E)). In addition, we have performed a time-course analysis of key serum biomarkers, measured at Day 9 and Day 18 during the 27-day treatment period. The results of these time-course measurements show no significant changes in these biomarkers at both time points, indicating that FMNQD treatment does not cause overt liver or kidney toxicity (Figure S17). These findings further confirm the biocompatibility of FMNQDs throughout the treatment period and provide a more thorough evaluation of the safety profile.

The results of pharmacokinetic properties of FMNQD show that FMNQD can remain in the blood for a relatively long time, with an average half-life ($T_{1/2}$) of 12.6 hours, and the area

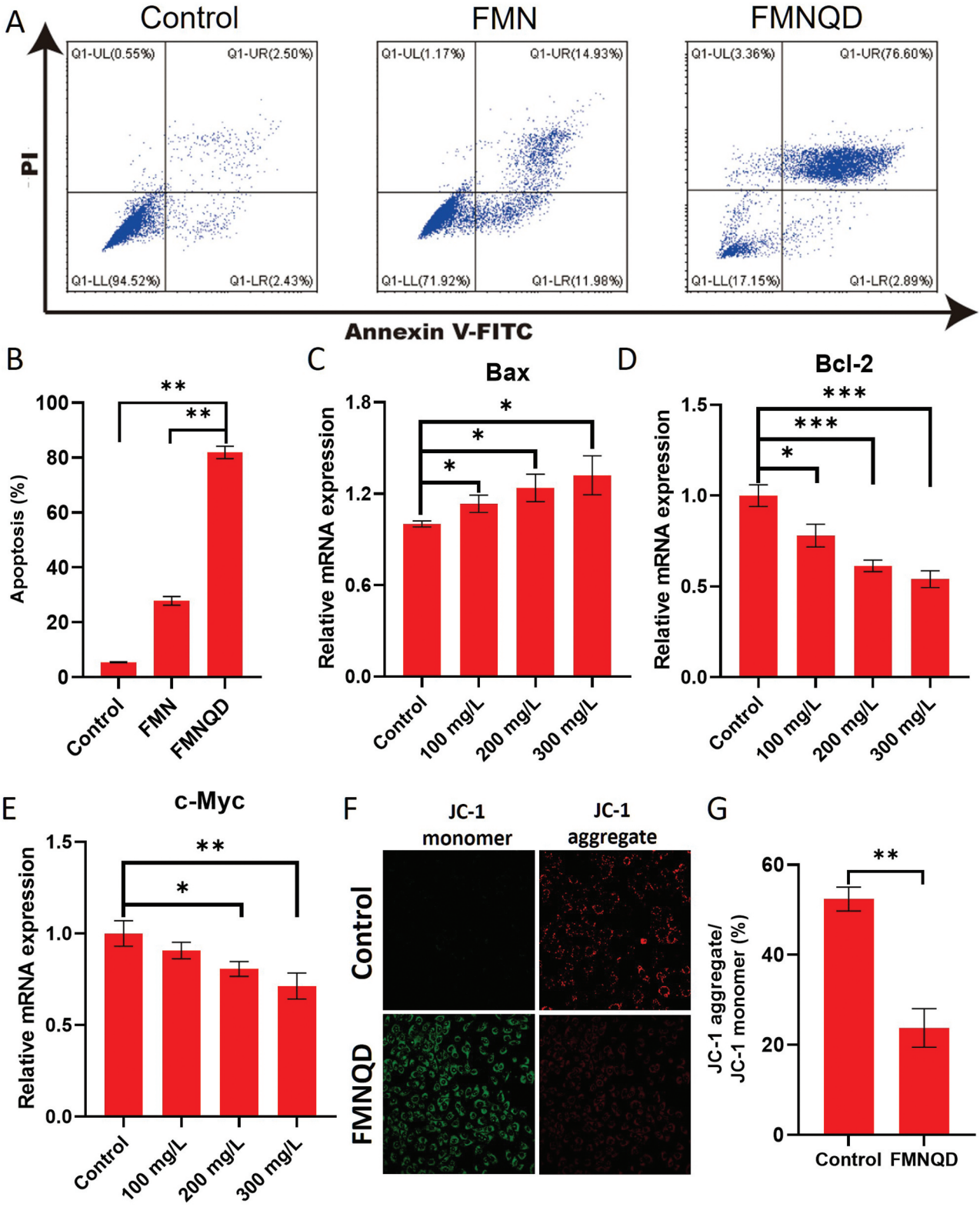

Figure 5. A) Analyze the apoptosis of SW620 cells after different treatments by using Annexin V-FITC and PI staining apoptosis kit by flow cytometry. B) Quantification of the percentage of apoptosis in SW620 cells after different treatments. C-E) qRT-PCR analysis of Bax, Bcl-2 and c-Myc. F) The JC-1 probe was used to stain SW620 cells with different treatments, and the changes of cell MMP were observed by CLSM. G) Statistical analyses of the relative ratio of JC-1 aggregate/JC-1 monomer. n = 3 per group. *$p < 0.05$, **$p < 0.01$ and ***$p < 0.01$.

under the curve (AUC) of the concentration over time is 183.5 mg L^{-1} h^{-1} (Figure S1B and Table S1). Regarding the metabolism and clearance of FMNQDs, our results indicate that FMNQDs are efficiently cleared from the body, with 79.5% of the administered dose being metabolized and excreted within 72 hours (Figure S18). This suggests that FMNQDs undergo rapid metabolic clearance, primarily through renal excretion, and have a relatively short elimination half-life. These findings

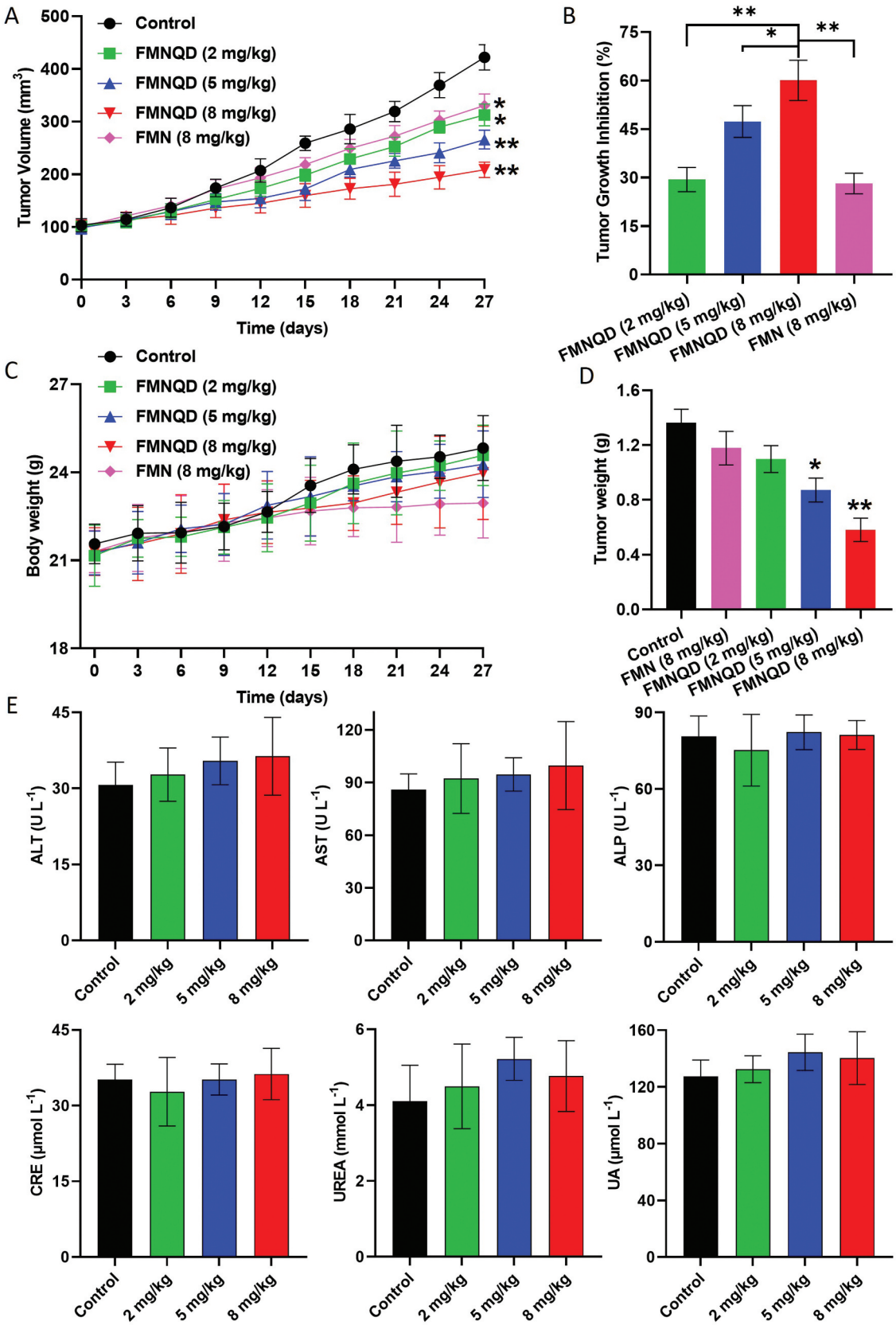

Figure 6. In *vivo* antitumor efficacy and toxicological evaluation. A) Tumor volume of mice (n = 6). B) Tumor inhibition rate (n = 6). C) Body weight changes (n = 6). D) The weight of tumor (n = 6). E) Evaluation of serum biochemistry after different treatments. $^{**}p < 0.01$ and $^{*}p < 0.05$.

Abbreviations: ALT: alanine aminotransferase, AST: aspartate aminotransferase, ALP: alkaline phosphatase, CRE: creatinine, UREA: urea nitrogen, UA: uric acid.

contribute to a better understanding of the pharmacokinetics of FMNQDs, confirming that they are effectively metabolized and rapidly cleared, which is important for their safe and effective use in nanomedicine.

4. Discussion

Formononetin (FMN) is an isoflavone from the phytoestrogen group, and in the field of medicine, this active compound has shown potential in the prevention and treatment of a wide range of diseases, including chronic conditions such as cancer, obesity and neurodegenerative diseases [20]. However, it has limited bioavailability, high permeability, and poor solubility (solubility in water was found to be 0.56 μg/mL [21]) because FMN is classified as biopharmaceutics class II [22]. To solve the above problems, based on FMN that is the natural antitumor agent, we synthesized a formononetin quantum dots (FMNQDs) for colon cancer therapy, which was prepared by PEGylation of FMN followed by hydrothermal reaction with urea and citric acid. TEM analysis showed that FMNQD had good dispersibility, and most of them were in a monodisperse state with a particle size of 2.03 ± 1.0 nm. The successful preparation of FMNQD was also confirmed by UV-vis, fluorescence spectrophotometer, and FTIR analyses. In addition, when the mass concentration was 0.2 mg/mL, under the condition of neutral medium, the fluorescence intensity of FMNQD was the highest, and it can stably exist in various metal ions (Ba^{2+}, Ca^{2+}, K^{+}, Mg^{2+}, Na^{+}, and Zn^{2+}), and has good stability and the ability to resist external ion interference.

In *vitro* fluorescence imaging showed that FMNQD can enter the cell through the cell membrane and is distributed in the cytoplasm, partly near mitochondria but mostly near lysosomes, indicating that the FMNQD is an acceptable fluorescent imaging material. CCK-8 assay results showed that cell viability gradually decreased with the increase of FMNQD concentration, and the inhibitory effect of the same concentration of FMNQD was stronger than that of FMN at the same time. This enhanced efficacy could be attributed to the nanoparticle's ability to facilitate drug internalization through endocytic pathways, potentially improving cellular uptake efficiency [23]. This improved cellular uptake can lead to higher intracellular drug concentrations and stronger cytotoxicity.

We next investigated the therapeutic mechanism of FMNQD in SW620 cells. Studies have demonstrated that drugs have the potential to induce apoptosis in tumor cells by augmenting the levels of intracellular ROS, which in turn modulate downstream cellular signaling pathways [3,24]. Our results indicate that FMNQD promotes tumor cell apoptosis and suppresses growth by elevating intracellular ROS levels. Given that apoptosis may be induced through the mitochondrial pathway, we plan to explore lysosomal escape strategies in the future to improve the mitochondrial delivery of FMNQDs. For example, using pH-sensitive or cationic coatings, these coatings can facilitate the release of FMNQDs from the lysosomes and direct them toward the mitochondria, thereby enhancing the therapeutic potential of FMNQDs. FMN has been reported to inhibit the growth of colon cancer cells and induce apoptosis, which is associated with caspase activation and reduced levels of Bcl-2 and Bax proteins [25]. Meanwhile, qRT-PCR analysis also confirmed that FMNQD could promote apoptosis and inhibit tumor cell growth. The results showed that FMNQD significantly increased the expression of pro-apoptotic gene Bax, decreased the expression of apoptosis inhibitor gene Bcl-2, and decreased the expression of cell proliferation-related gene c-Myc compared with the control group. Bax, an important pro-apoptotic gene, is a key executioner of mitochondrial regulation of cell death through its lethal activity of permeabilizing the mitochondrial outer membrane (MOM) [26]. Bcl-2 has been identified as an effective regulator of apoptosis, a proto-oncogene that inhibits apoptosis by preventing mitochondrial permeability [27]. c-Myc, a well-established oncogene, plays a vital role in the initiation and progression of various cancers [28]. In addition, in many instances, mitochondria are crucial for the initiation of apoptosis, which is closely related to its dysfunction [29]. Our data suggest that FMNQD significantly reduced MMP.

In *vivo* studies confirmed FMNQD significantly suppressed colon cancer progression, the tumor inhibition rate of 8 mg/kg group was 60.06 ± 6.22%. The analysis results of serum biomarkers of the liver and kidneys confirmed the therapeutic safety of FMNQD.

5. Conclusion

In this study, based on FMN that is the natural antitumor agent, we synthesized FMNQDs for colon cancer therapy, which was prepared by PEGylation of FMN followed by hydrothermal reaction with urea and citric acid. FMNQD has good dispersibility and a particle size of 2.03 ± 1.0 nm, which can be stably existed in various metal ions (Ba^{2+}, Ca^{2+}, K^{+}, Mg^{2+}, Na^{+}, Zn^{2+}) solution, and has good intracellular fluorescence imaging effect. Most important of all, FMNQD increased intracellular ROS production, reduces MMP, increases the expression of pro-apoptotic genes Bax and caspase-3, and down-regulates the anti-apoptotic gen Bcl-2 expression, and simultaneously increased the expression of autophagy marker LC3-II and decreased the expression of p62. These findings indicate that FMNQD induces tumor cell death through mitochondrial-mediated apoptotic pathways and autophagic pathways. In *vivo*, it significantly inhibited tumor growth with no observed toxicity. Despite these promising results, this study has some limitations, such as the lack of long-term stability and biodegradation studies of FMNQDs in *vivo*, and the need for more comprehensive molecular analyses to further elucidate their mechanisms of action. Future research should explore the combination of FMNQDs with other therapeutic modalities, such as immunotherapy, to enhance their antitumor efficacy, and investigate their potential in targeted drug delivery systems, offering a promising approach for personalized cancer treatment.

Funding

This study was supported by the Scientific Research Foundation for High-level Talents of Anhui University of Science and Technology [2024yjrc92], the National Natural Science Foundation of China [82502551], the Anhui Provincial Natural Science Foundation [2508085QH330], the Postdoctoral Fellowship Program of CPSF [GZB20250676], and the Postdoctoral Research Funding Project of Anhui Province [2024C887].

CRediT authorship contributions statement

Junfeng Zhang: Investigation, Data curation, Funding acquisition, Writing – original draft. Yuqing Cui: Validation, Investigation, Writing – original draft. Chenchen Li: Validation, Methodology. Tongjin Yin: Supervision, Methodology, Investigation. Min Xu: Investigation, Conceptualization, Writing – original draft. Hongliang Bian: Supervision, Methodology, Writing – review & editing.

Disclosure statement

The authors have no relevant affiliations or financial involvement with any organization or entity with a financial interest in or financial conflict with the subject matter or materials discussed in the manuscript. This includes employment, consultancies, honoraria, stock ownership or options, expert testimony, grants or patents received or pending, or royalties.

No writing assistance was utilized in the production of this manuscript.

Reviewer disclosures

Peer reviewers on this manuscript have no relevant financial or other relationships to disclose.

Data availability statement

The data that support the findings of this study are available from the corresponding author upon reasonable request.

References

1. Kong MY, Li LY, Lou YM, et al. Chinese herbal medicines for prevention and treatment of colorectal cancer: from molecular mechanisms to potential clinical applications. J Integr Med. 2020;18(5):369–384. doi: 10.1016/j.joim.2020.07.005
2. Lannagan TR, Jackstadt R, Leedham SJ, et al. Advances in colon cancer research: in vitro and animal models. Curr Opin Genet Dev. 2021;66:50–56. doi: 10.1016/j.gde.2020.12.003
3. Zhang J, Li C, Xue Q, et al. An efficient carbon-based drug delivery System for cancer therapy through the nucleus targeting and mitochondria mediated apoptotic pathway. Small Methods. 2021;5(12):e2100539. doi: 10.1002/smtd.202100539
4. Hui B, Zhou C, Xu Y, et al. Exosomes secreted by fusobacterium nucleatum-infected colon cancer cells transmit resistance to oxaliplatin and 5-FU by delivering hsa_circ_0004085. J Nanobiotechnol. 2024;22(1):62. doi: 10.1186/s12951-024-02331-9
5. Hamze K, Abdallah RH, Younis NK, et al. 2-nucleobase-substituted 4,6-diaminotriazine analogs: synthesis andAnti-cancer activity in 5-fluorouracil-sensitive and resistant ColorectalCancer cells. Curr Med Chem. 2023;30(26):3032–3049. doi: 10.2174/0929867329666220914112042
6. Xie S, Zhou Z, Zheng Y, et al. Novel drug research and therapeutic strategies targeting tumor metastasis and cancer stem cells. Front Pharmacol. 2025;16:1643183. doi: 10.3389/fphar.2025.1643183
7. Al Zein M, Boukhdoud M, Shammaa H, et al. Immunotherapy and immunoevasion of colorectal cancer. Drug Discov Today. 2023;28(9):103669. doi: 10.1016/j.drudis.2023.103669
8. Chibaya L, Snyder J, Ruscetti M. Senescence and the tumor-immune landscape: implications for cancer immunotherapy. Semin Cancer Biol. 2022;86(Pt 3):827–845. doi: 10.1016/j.semcancer.2022.02.005
9. Sun D, Hadjiiski L, Bruno G, et al. Evaluating the reliability of large language models for clinical data extraction in bladder cancer prognosis. Sci Rep. 2025;15(1). doi: 10.1038/s41598-025-27593-7
10. Kurosaki T, Okada A, Takashima Y, et al. Biodegradable nanoparticles encapsulating murine Double minute 2 siRNA to treat peritoneal dissemination of colon cancer. Int J Mol Sci. 2025;26(18):8883. doi: 10.3390/ijms26188883
11. Iravani S, Varma RS. Green synthesis, biomedical and biotechnological applications of carbon and graphene quantum dots. A Rev Environ Chem Lett. 2020;18(3):703–727. doi: 10.1007/s10311-020-00984-0
12. Ong SKL, Shanmugam MK, Fan L, et al. Focus on Formononetin: anticancer potential and molecular targets. Cancers (basel). 2019;11(5):611. doi: 10.3390/cancers11050611
13. Aliya S, Alhammadi M, Park U, et al. The potential role of formononetin in cancer treatment: an updated review. Biomed Pharmacother. 2023;168:115811. doi: 10.1016/j.biopha.2023.115811
14. Almatroodi SA, Almatroudi A, Khan AA, et al. Potential therapeutic targets of Formononetin, a type of methoxylated isoflavone, and its role in cancer therapy through the modulation of signal transduction pathways. Int J Mol Sci. 2023;24(11):9719. doi: 10.3390/ijms24119719
15. Zhang X, Li Q, Wang J, et al. Physicochemical properties and in vitro release of formononetin nano-particles by ultrasonic probe-assisted precipitation in four polar organic solvents. Food Chem. 2024;461:140918. doi: 10.1016/j.foodchem.2024.140918
16. Hwang CY, Han YH, Lee SM, et al. Sestrin2 attenuates cellular senescence by inhibiting NADPH oxidase 4 expression. Ann Geriatr Med Res. 2020;24(4):297–304. doi: 10.4235/agmr.20.0051
17. Abu-Fayyad A, Nazzal S. Synthesis, physiochemical characterization, and in vitro antitumor activity of the amide and pH cleavable hydrazone conjugates of γ-tocotrienol isomer of vitamin E with methoxy-poly(ethylene) glycol. Int J Pharm. 2017;529(1–2):75–86. doi: 10.1016/j.ijpharm.2017.06.033
18. Li Y, Su J, Liu S, et al. Improved stability and biocompatibility of lycopene liposomes with sodium caseinate and PEG coating. Int J Biol Macromol. 2025;311(Pt 2):143685. doi: 10.1016/j.ijbiomac.2025.143685
19. Yin L, Pang Y, Shan L, et al. The in vivo pharmacokinetics of block copolymers containing polyethylene glycol used in nanocarrier drug delivery systems. Drug Metab Dispos. 2022;50(6):827–836. doi: 10.1124/dmd.121.000568
20. Machado Dutra J, Espitia PJP, Andrade Batista R. Formononetin: biological effects and uses - a review. Food Chem. 2021;359:129975.
21. Wang Y, Deng Z, Wang X, et al. Formononetin/methyl-β-cyclodextrin inclusion complex incorporated into electrospun polyvinyl-alcohol nanofibers: enhanced water solubility and oral fast-dissolving property. Int J Pharm. 2021;603:120696. doi: 10.1016/j.ijpharm.2021.120696
22. Zou Z, Xue Y, Adu-Frimpong M, et al. Formononetin-loaded self-microemulsion drug delivery systems for improved solubility and oral bioavailability: fabrication, characterization, *in vitro* and *in vivo* evaluation. Pharm Sci Tech. 2024;25(8):261. doi: 10.1208/s12249-024-02975-8
23. Sousa de Almeida M, Susnik E, Drasler B, et al. Understanding nanoparticle endocytosis to improve targeting strategies in nanomedicine. Chem Soc Rev. 2021;50(9):5397–5434. doi: 10.1039/D0CS01127D
24. Zhu B, Li Y, Lin Z, et al. Silver nanoparticles induce HePG-2 cells apoptosis through ROS-Mediated signaling pathways. Nanoscale Res Lett. 2016;11(1):198. doi: 10.1186/s11671-016-1419-4
25. Hu Y, Zhai W, Tan D, et al. Uncovering the effects and molecular mechanism of Astragalus membranaceus (Fisch.) Bunge and its bioactive ingredients formononetin and calycosin against colon cancer: an integrated approach based on network pharmacology analysis coupled with experimental validation and molecular docking. Front Pharmacol. 2023;14:1111912.
26. Spitz AZ, Gavathiotis E. Physiological and pharmacological modulation of BAX. Trends Pharmacol Sci. 2022;43(3):206–220. doi: 10.1016/j.tips.2021.11.001
27. Youle RJ, Strasser A. The BCL-2 protein family: opposing activities that mediate cell death. Nat Rev Mol Cell Biol. 2008;9(1):47–59. doi: 10.1038/nrm2308
28. Ge J, Yu W, Li J, et al. USP16 regulates castration-resistant prostate cancer cell proliferation by deubiquitinating and stablizing c-Myc. J Exp Clin Cancer Res. 2021;40(1):59. doi: 10.1186/s13046-021-01843-8
29. Bock FJ, Tait SWG. Mitochondria as multifaceted regulators of cell death. Nat Rev Mol Cell Biol. 2020;21(2):85–100. doi: 10.1038/s41580-019-0173-8